JOURNAL OF SOLID STATE CHEMISTRY **125,** 261–269 (1996)
ARTICLE NO. 0295

Structural Features of the Reactives Sites in α-$M(DPO_4)_2 \cdot D_2O$ (M = Ti, Zr, Pb): Hydrogen-Bond Network and Framework

Enrique R. Losilla, Miguel A. G. Aranda, and Sebastian Bruque

Departamento de Química Inorgánica, Cristalografía y Mineralogía, Universidad de Málaga, Aptd. 59, 29071 Málaga, Spain

Received April 1, 1996; in revised form June 13, 1996; accepted June 17, 1996

Three crystalline layered metal (IV) acid phosphates α-$M(DPO_4)_2 \cdot D_2O$, α-MP, (M = Zr, Ti, Pb) have been hydrothermally synthesized and the size and shape of the microparticles have been analyzed by the Scherrer method. The crystal structures of α-ZrP and α-TiP have been refined from a combined X-ray and neutron powder diffraction study by the Rietveld method. These hydrogen phosphates are isomorphous and belong to the α-ZrP-type structure. However, this precise powder diffraction study has shown that the frameworks and hydrogen-bond networks of these materials are slightly different. The unit cell volume of α-ZrP is larger than that of α-TiP because the layers in α-ZrP are less corrugated than those in α-TiP. The H-bond network is also slightly different, as in α-ZrP there is not H bonding between the layers, the shortest contact being O(7) ··· D(4) of 2.56(3) Å. For α-TiP this contact is much shorter, 2.33(2) Å, which may indicate a small but not negligible H-bond interaction between layers. Moreover, the intralayer H bonds are weaker in α-ZrP than in α-TiP as evidenced in the O(4) ··· D(3) interactions of 2.41(3) and 2.16(2) Å, respectively.

INTRODUCTION

Acidic materials based on layered hydrogen phosphates of metals(IV) of composition $M(HPO_4)_2 \cdot H_2O$ (M = Si, Ge, Sn, Pb, Ti, Zr, Hf) constitute an isostructural series, α-MP. Only α-ZrP has been structurally characterized by single crystal X-ray diffraction (1, 2). Neutron powder diffraction studies on α-ZrP have also been carried out (3, 4), however the precision on the reported structural data were low. Other structural studies with powder data have shown that for M = Ti (5) and Hf (6) the frameworks are similar to that of zirconium analog although the precision of the reported data was quite low, probably due to the low degree of crystallinity of the synthesized products.

The structure of α-ZrP is very well known (2) and is built up of layers of slightly distorted ZrO_6 octahedra and alternating (up and down) HPO_4 tetrahedra. These layers have a pseudo-hexagonal symmetry and are stacked along the c-axis. The water molecules are located in the interlayer space and participate in the hydrogen-bond network (3, 4). The hydrogen atom positions, although with large errors, were derived from this powder neutron study. One hydrogen of the water acts as donor in one H bond with the oxygen of a neighboring POH group. The other water hydrogen does not participate in H bonding. Both crystallographically independent acidic POH groups in the same layer form hydrogen bonds with the oxygen of the water molecule. The layers are only bound by van der Waals forces. There are no neutron diffraction studies for other members of the series. Therefore, it has been assumed, so far, that the hydrogen bond network is similar in all the series.

We recently reported a preliminary structural study of α-MP, (M = Ti, Sn, Pb, Zr) based on X-ray powder diffraction (7). As a result of that study we concluded that the unit cell of α-ZrP is larger than those of the other members of the series. However, some results were not conclusive as the derived parameters had large errors. It is important to know the structural differences and similarities between α-ZrP and the other members of the series and to understand the H-bond network, as these materials are used as acid solids (8), ion exchangers (9), sensors (10), and host materials for intercalation reactions (11, 12).

The structures are quite complex, with 16 atoms in the asymmetric part of the unit cell, and we have therefore carried out a combined powder X-ray and neutron diffraction study of α-ZrP and α-TiP to obtain a detailed picture of the structures. This has allowed us to understand the structural differences between α-ZrP and other members of the series in the framework and the H-bond network.

EXPERIMENTAL

Synthesis

Deuterated powdered α-MP samples were synthesized under hydrothermal conditions. The starting compounds were D_3PO_4 (85% w/w, 99+% D, Aldrich-Chemie), D_2O (99.8% D, Merck), and reactive anhydrous metal oxides synthesized as described below.

0022-4596/96 $18.00

Zr and Ti oxides were synthesized by slow hydrolysis of alcoholic metal alkoxide solutions ($Zr(OCH_2CH_2CH_3)_4$ 70% and $Ti[OCH(CH_3)_2]_4$ 97%). The white suspensions were thoroughly washed with water and heated at 300°C for 2 h. X-ray powder patterns showed amorphous powders and IR spectra indicated that these metal oxides were anhydrous. PbO_2 (Probus, analytical grade) was used as source of lead, and it was heated to remove the adsorbed water.

Hydrothermal syntheses of α-MP (M = Zr, Ti) were carried out in a Teflon-lined PARR bomb with a free volume of 45 ml. $Zr(DPO_4)_2 \cdot D_2O$ was obtained by heating a mixture of 3 g of ZrO_2, 15 g of D_3PO_4, and 10 g of D_2O, at 165°C for 7 days. $Ti(DPO_4)_2 \cdot D_2O$ was obtained by heating a mixture of 2 g of TiO_2, 15 g of D_3PO_4, and 10 g of D_2O, at 150°C for 7 days. In both cases the overall reactive molar ratios, $M:P:D_2O$, were 1:5:30.

$Pb(DPO_4)_2 \cdot D_2O$ was hydrothermally synthesized in a Teflon-lined BERGOFF reactor with a gas inlet and magnetic stirring. The starting compounds were 2.51 g of PbO_2 and 50 g of D_3PO_4 which result in an overall reactive molar ratio $M:P:D_2O$, of 1:40:40. Before heating, the air was removed and a pressure of 40 bar of O_2 was introduced in the reactor to avoid the reduction of the Pb(IV). Then, the temperature was increased to 120°C for 6 days.

The three resulting white solids were centrifuged and washed with 10 ml of D_2O, and two times with 30 ml of dried acetone. The solids were kept in a dessicator over KOH and a glass with 5 ml of D_2O. The X-ray powder diffraction patterns indicated the presence of highly crystalline single phases.

Powder Diffraction

Neutron powder diffraction patterns were recorded on D1A diffractometer at ILL neutron source. The experimental conditions were: wavelength, 1.909 Å; useful 2Θ range 12°–140°, step size 0.05° (in 2Θ), counting for a day to record a high quality pattern. Three days were used to collect the patterns for α-MP (M = Zr, Ti, Pb). X-ray diffraction patterns for the same samples were recorded on a Siemens D501 automated diffractometer using graphite-monochromated Cu$K\alpha$ radiation, 1.5418 Å. The data were collected in the Bragg–Brentano ($\Theta/2\Theta$) geometry (reflection mode). The experimental conditions were: 2Θ range 15°–120°, step size 0.05° (in 2Θ), counting time 15 s, ≈9 h. The data were fitted by the Rietveld method (13) using the GSAS suite of programs (14). The pseudo-Voigt function corrected for asymmetry at low angles was used to simulate the peak shape for both sets of patterns. The background was fitted through a Fourier series by refining five terms.

The X-ray patterns were indexed on monoclinic unit cells, space group $P2_1/n$, with dimensions: a = 9.066 Å, b = 5.294 Å, c = 15.447 Å, and β = 101.69° for α-ZrP; a = 8.640 Å, b = 5.009 Å, c = 15.510 Å, and β = 101.32° for α-TiP; and a = 8.624 Å, b = 4.987 Å, c = 16.125 Å, and β = 100.61° for α-PbP.

RESULTS

We have determined the average size of the microcrystals of these materials from the X-ray powder data, and the crystal structures have been reanalyzed by the Rietveld method. GSAS allows refinement of a set of structural parameters against different data sets, and in this case we have used neutron and X-ray powder diffraction data. The previously determined structures of α-ZrP (2), α-TiP, and α-PbP (7) have been used as starting models for the refinements. Initial hydrogen positions were taken from the previous neutron study (3) although they were confirmed by difference Fourier maps for each sample.

First, we refined the overall parameters for both data sets: background parameters, histogram scale factors, zero shift errors, unit cell parameters, and peak shape parameters for the pseudo-Voigt function. The refinements resulted in quite good fits. At this stage, sample dependent problems were attacked. These compounds are lamellar and the microparticles grow as plaques being longer along the a and b directions (parallels to the layers) than along the c-axis (perpendicular to the layers), hence preferred orientation may be expected. We checked for this phenomenon and it was present only in the X-ray patterns. Neutron patterns did not present it as the samples were loaded into the cylindrical vanadium can without any pressing. However, to get a flat surface for the X-ray experiment the sample has to be pressed on the aluminium holder, resulting in preferred orientation. GSAS can model this effect, through the March–Dollase correction (15), and the fit was slightly improved. Due to the shape of the microparticles, described above, anisotropic peak broadening may also be expected. This phenomenon was observed in both data sets, as the (hk0) peaks were slightly sharper than the (hkl) peaks with $l \neq 0$. These can also be modeled with GSAS, resulting in slightly better fits. No absorption correction was necessary for the neutron data.

Second, the atomic parameters were refined: positional parameters, isotropic temperature factors, and D/H ratios. We had to refine the deuterium/hydrogen ratios as the samples were not fully deuterated. To avoid correlations, one isotropic temperature factor and one deuterium/hydrogen ratio was refined for each deuterium type (deuterium of the hydrogen phosphate group and of the water molecule).

The average anisotropic microparticle sizes (for α-ZrP, α-TiP, and α-PbP) were determined by the Scherrer method (16) from the overall Lorentzian peak shape parameters obtained in the refinements of the X-ray patterns

TABLE 1
Peak Shape Parameters and Average Microparticle Sizes for α-MP (M = Zr, Ti, Pb)

	Zr	Ti	Pb
GW[a]/° × 10^2	37.8(6)	46.5(7)	89(4)
LX[a]/° × 10^2	5.3(1)	5.0(1)	4.8(4)
STEC[a]/° × 10^2	8.9(6)	6.2(5)	59(3)
P_{ab}[b]/Å ≈	830(20)	880(20)	910(70)
P_c[b]/Å ≈	310(15)	390(15)	70(5)

[a] Lorentzian peak shape parameters in GSAS (defined in Ref. 14).
[b] Particle diameters along the crystallographic directions given. Calculated from the Lorentzian peak shape parameters.

(14) and are given in Table 1. Final observed, calculated, and difference profiles for α-ZrP and α-TiP are shown in Figs. 1–4. Results of the combined powder diffraction study are given in Table 2. Structural parameters are given in Table 3 and selected framework bond distances and angles are given in Table 4. Distances and angles around the water molecule are given in Table 5. The observed, calculated, and difference profiles for α-PbP are shown in Fig. 5.

DISCUSSION

Microparticles Study

The refinements of the neutron patterns gave similar refined values for the Lorentzian peak shape parameters to those from the X-ray study. However, they were affected by a larger error because the neutron diffraction peaks are wider, due to a larger Gaussian contribution to the peak shape. Hence the reported anistropic sizes of the microcrystals (Table 1) are those obtained from the X-ray patterns.

Hydrothermal syntheses led to microcrystals well developed (≈900 Å) along the *ab* plane. However, along the *c*-axis direction (perpendicular to the layer) the size of the microcrystals were smaller. Although the temperature of the synthesis for α-ZrP, 165°C, was higher than that for α-TiP, 150°C, the size of the microcrystals along the *c*-axis for α-ZrP was slightly smaller than that for α-TiP (see Table 1). This is explained because the reactivity of the ZrO_2 oxide precursor is smaller than that of the titanium analog. It is worthy of mention that commercial crystalline ZrO_2 of small particle size (Alfa, 99+, 1–3 μm) does not react under the hydrothermal conditions given in the Experimental.

To synthesize α-PbP, low temperature is necessary in order to avoid partial reduction of Pb(IV) to Pb(II). This low temperature, 120°C, results in a very small particle size along the direction perpendicular to the layers, although along the layer directions the crystals are well developed (Table 1). Under mild conditions, the crystals grow fast in the *ab* plane and more temperature and time is necessary to grow along the *c*-axis. However, both variables act against the chemical stability of α-PbP.

The crystallinity and reactivity of these materials have been a matter of much interest as they can be prepared in a wide range of crystallinity depending upon the synthesis conditions. The crystallinity (the microparticle sizes and shapes) has important implications on the reactivity and stability of these materials.

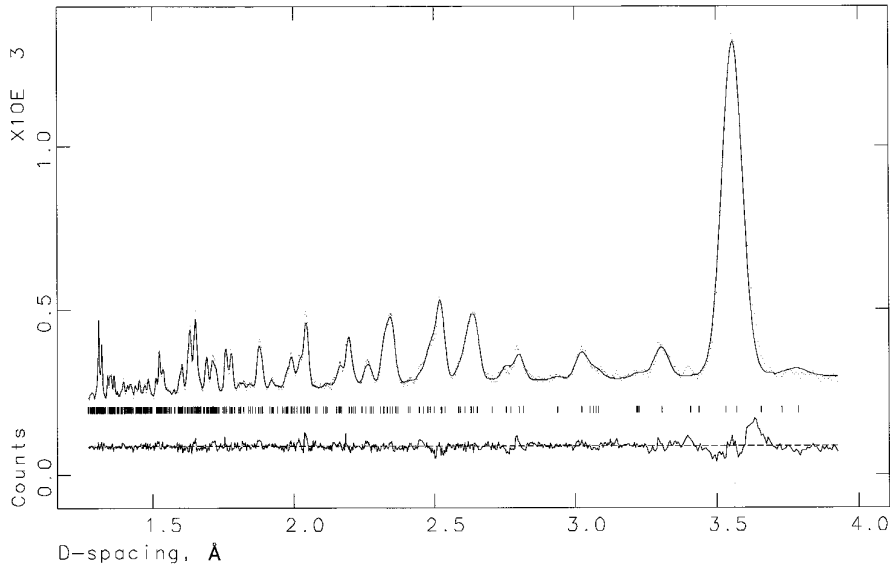

FIG. 1. Final observed (points), calculated (full line), and difference neutrons (λ = 1.909 Å) profiles for α-$Zr(DPO_4)_2 \cdot D_2O$. Allowed reflection marks are also shown.

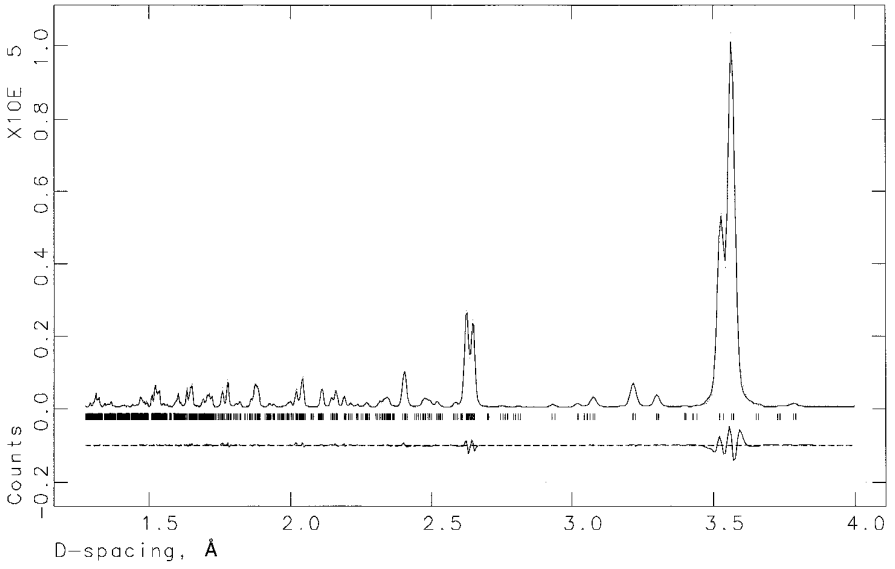

FIG. 2. Final observed (points), calculated (full line), and difference X-ray (λ = 1.5418 Å) profiles for α-$Zr(DPO_4)_2 \cdot D_2O$. Allowed reflection marks are also shown.

Structural Study

The refinement of a complex crystal structure against different data sets (X-ray and neutrons) obviously reduced the systematic errors in powder diffraction studies, resulting in more accurate structural parameters. The complementary information that can be extracted from both data sets is also important. Light element positions (hydrogen/deuterium) can be easily deduced from the neutron data, and the contribution of heavy cations is stronger in the X-ray patterns.

In this study, we have used the same step size (0.05/2Θ) for both patterns (X-ray and neutron) in order to not overweight the X-ray data in the refinement. The decrease of the step size (adding more points to the refinements) results in a decrease of the standard deviations but this does not reflect increased accuracy of the refinement.

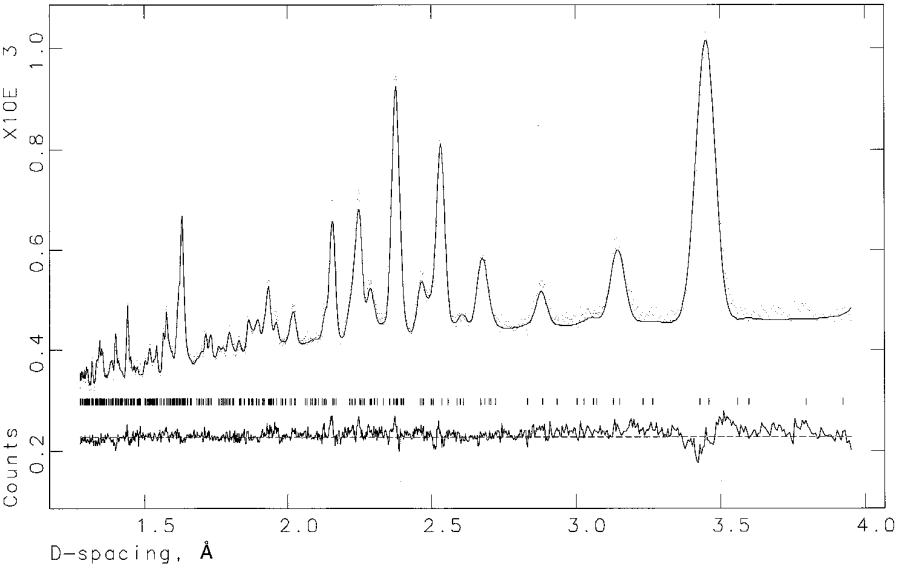

FIG. 3. Final observed (points), calculated (full line), and difference neutrons (λ = 1.909 Å) profiles for α-$Ti(DPO_4)_2 \cdot D_2O$. Allowed reflection marks are also shown.

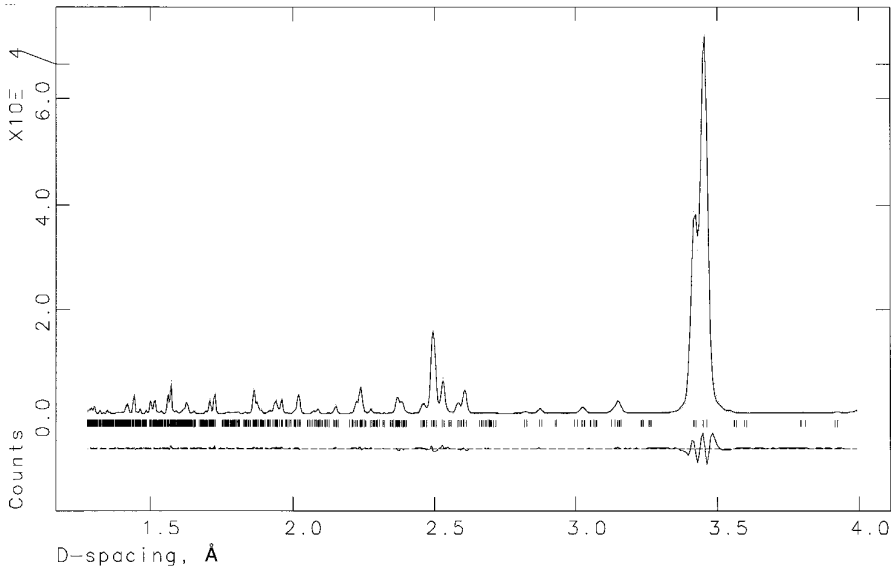

FIG. 4. Final observed (points), calculated (full line), and difference X-ray (λ = 1.5418 Å) profiles for α-$Ti(DPO_4)_2 \cdot D_2O$. Allowed reflection marks are also shown.

The samples were highly deuterated. For α-TiP, the refinement converged to 83(2)% deuterium for the hydrogen phosphate groups and 81(2)% deuterium for the water molecule. For α-ZrP, these values were 88(4) and 96(4)%, respectively. In this last case, a slight correlation between the D/H ratios and their temperature factors (Table 1) was detected, which increases the errors in both type of parameters. However, this correlation does not affect the deuterium position and, hence, the H-bond network discussed below.

TABLE 2
Some Results for the Combined X-Ray and Neutron Powder Diffraction Study for α-MP (M = Zr, Ti) in the Space Group $P\,2_1/n$

	Unit cell parameters			
	a/Å	b/Å	c/Å	β/°
α-ZrP refinement	9.0683(2)	5.2929(1)	15.4562(4)	101.727(1)
α-TiP refinement	8.6358(2)	5.0083(3)	15.4993(3)	101.338(1)
	Zr–N pattern	Zr–RX pattern	Ti–N pattern	Ti–RX pattern
λ/Å	1.909	1.5418	1.909	1.5418
Prefer orientation	—	0.960(2)	—	0.935(2)
No. hkl reflcn.	687	1066	637	975
R_{WP} (%)	5.7	7.8	5.4	7.5
R_P (%)	2.5	3.1	2.1	2.5
R_F (%)	4.3	3.0	7.2	3.1
$R_{WP}^{overall}$ (%)	5.6		4.2	

TABLE 3
Refined Atomic Parameters for α-TiP and α-ZrP

Atom		x	y	z	B(Å^2)
M	Ti–NXPD	0.24664(23)	0.2524(10)	0.48719(11)	0.42(4)
	Zr–NXPD	0.24586(17)	0.2537(9)	0.48535(8)	0.56(3)
P(1)	Ti–NXPD	0.3898(4)	0.7529(13)	0.39274(17)	0.69(7)
	Zr–NXPD	0.3882(5)	0.7509(22)	0.38589(23)	0.81(8)
P(2)	Ti–NXPD	−0.13001(35)	0.2430(12)	0.40125(17)	0.53(6)
	Zr–NXPD	−0.1325(4)	0.2457(22)	0.39756(23)	0.74(8)
O(1)	Ti–NXPD	0.5526(7)	0.8334(14)	0.4389(4)	0.94(16)
	Zr–NXPD	0.5451(9)	0.8075(21)	0.4391(5)	0.62(22)
O(2)	Ti–NXPD	0.3456(7)	0.4668(14)	0.4103(4)	0.64(14)
	Zr–NXPD	0.3375(11)	0.4868(19)	0.4025(7)	0.74(22)
O(3)	Ti–NXPD	0.2659(8)	0.9481(15)	0.4126(5)	1.11(16)
	Zr–NXPD	0.2790(11)	0.9515(19)	0.4040(8)	0.58(23)
O(4)	Ti–NXPD	0.3813(6)	0.7583(20)	0.29069(31)	0.81(12)
	Zr–NXPD	0.3895(8)	0.7716(25)	0.2849(4)	0.59(17)
O(5)	Ti–NXPD	−0.2309(8)	0.4390(14)	0.4402(4)	0.99(15)
	Zr–NXPD	−0.2203(11)	0.4417(17)	0.4379(6)	0.34(22)
O(6)	Ti–NXPD	−0.1439(8)	−0.0431(14)	0.4368(4)	0.88(16)
	Zr–NXPD	−0.1499(11)	−0.0229(20)	0.4343(7)	1.66(27)
O(7)	Ti–NXPD	0.0408(7)	0.3384(13)	0.41553(32)	0.43(15)
	Zr–NXPD	0.0334(8)	0.3064(20)	0.4091(5)	0.27(22)
O(8)	Ti–NXPD	−0.1885(6)	0.2488(20)	0.30063(31)	1.19(13)
	Zr–NXPD	−0.1943(8)	0.2431(28)	0.2948(4)	0.67(16)
O(9)	Ti–NXPD	0.0043(8)	0.7136(15)	0.2629(4)	1.13(13)
	Zr–NXPD	0.0011(12)	0.7160(22)	0.2600(6)	2.21(20)
D(1)	Ti–NXPD	0.4204(20)	0.917(4)	0.2726(11)	3.04(34)
	Zr–NXPD	0.4290(22)	0.930(4)	0.2655(14)	2.37(49)
D(2)	Ti–NXPD	−0.2957(20)	0.2363(35)	0.2783(11)	3.04(−)
	Zr–NXPD	−0.3044(20)	0.236(4)	0.2755(11)	2.37(−)
D(3)	Ti–NXPD	0.0517(21)	0.874(4)	0.2528(14)	3.58(42)
	Zr–NXPD	0.0508(24)	0.854(5)	0.2596(20)	6.28(75)
D(4)	Ti–NXPD	0.0253(21)	0.703(4)	0.3212(11)	3.58(−)
	Zr–NXPD	0.0288(27)	0.722(6)	0.3238(14)	6.28(−)

TABLE 4
Framework Bond Distances and Angles for α-ZrP and α-TiP

	Zr	Ti		Zr	Ti
M–O(1)	2.040(8)	1.929(6)	*M*–O(5)	2.043(10)	1.932(8)
M–O(2)	2.070(11)	1.924(7)	*M*–O(6)	2.057(11)	1.920(8)
M–O(3)	2.093(12)	1.940(8)	*M*–O(7)	2.062(7)	1.950(6)
P(1)–O(1)	1.521(9)	1.502(6)	P(2)–O(5)	1.517(11)	1.514(8)
P(1)–O(2)	1.510(14)	1.521(9)	P(2)–O(6)	1.551(14)	1.548(8)
P(1)–O(3)	1.516(12)	1.524(8)	P(2)–O(7)	1.513(8)	1.525(7)
P(1)–O(4)	1.566(7)	1.569(5)	P(2)–O(8)	1.574(7)	1.542(5)
O(1)–*M*–O(2)	90.3(4)	92.0(3)	O(2)–*M*–O(7)	90.7(4)	89.4(3)
O(1)–*M*–O(3)	89.6(4)	90.4(3)	O(3)–*M*–O(5)	177.3(5)	178.5(4)
O(1)–*M*–O(5)	89.7(4)	89.5(3)	O(3)–*M*–O(6)	92.2(5)	92.3(4)
O(1)–*M*–O(6)	91.0(4)	89.1(3)	O(3)–*M*–O(7)	89.5(4)	90.5(3)
O(1)–*M*–O(7)	178.6(6)	178.3(3)	O(5)–*M*–O(6)	90.4(4)	89.2(3)
O(2)–*M*–O(3)	87.7(4)	88.2(3)	O(5)–*M*–O(7)	91.2(4)	89.7(3)
O(2)–*M*–O(5)	89.8(5)	90.3(4)	O(6)–*M*–O(7)	88.0(4)	89.5(3)
O(2)–*M*–O(6)	178.7(4)	178.8(4)			
O(1)–P(1)–O(2)	112.0(7)	114.3(5)	O(5)–P(2)–O(6)	112.1(7)	111.5(5)
O(1)–P(1)–O(3)	109.7(8)	111.1(5)	O(5)–P(2)–O(7)	113.5(8)	110.8(5)
O(1)–P(1)–O(4)	109.2(5)	109.2(4)	O(5)–P(2)–O(8)	108.2(8)	106.9(5)
O(2)–P(1)–O(3)	112.6(7)	110.9(5)	O(6)–P(2)–O(7)	108.9(7)	112.3(5)
O(2)–P(1)–O(4)	107.4(8)	103.5(5)	O(6)–P(2)–O(8)	108.6(9)	110.1(6)
O(3)–P(1)–O(4)	105.8(8)	107.3(5)	O(7)–P(2)–O(8)	105.2(5)	104.8(4)
M–O(1)–P(1)	159.4(9)	150.6(5)	*M*–O(5)–P(2)	155.5(7)	149.6(5)
M–O(2)–P(1)	146.3(7)	142.6(5)	*M*–O(6)–P(2)	148.5(7)	143.2(5)
M–O(3)–P(1)	145.5(7)	140.4(5)	*M*–O(7)–P(2)	146.1(6)	139.6(4)

Unfortunately, there was a problem in the synthesis of the lead hydrogen phosphate that resulted in a poorly deuterated sample. Due to the low degree of deuteration and to the small particle size along the *c*-axis, the neutron data was of insufficent quality to derive good structural parameters. As the aim of this work is to analyze precisely the crystal structures of these phosphates, the combined neutron and X-ray study for the lead compound will not be reported.

Framework of α-MP series. The structural results for α-ZrP are essentially identical to those previously reported from single crystal data (2). All framework positional parameters obtained in this study (Table 3) agree, within 3–4 standard deviations, with the single crystal values. The refinement for α-TiP converged to a very similar structure. MO_6 octahedra and PO_4 tetrahedra are regular as deduced from the distances and angles given in Table 4. It is worth pointing out that P–O bond distances to the oxygen of the

TABLE 5
Distances and Angles Around the Water Molecules for α-ZrP and α-TiP

	Zr–NXPD	Zr–NPD	Ti–NXPD		Zr–NXPD	Zr–NPD	Ti–NXPD
O(4)–D(1)	0.982(20)	0.91(7)	0.930(18)	O(8)–D(2)	0.983(17)	1.05(6)	0.925(16)
O(9)–D(3)	0.860(26)	0.94(7)	0.927(20)	O(9)–D(4)	0.968(23)	0.92(5)	0.887(17)
O(9) ··· D(1)[a]	1.718(23)	1.92(7)	1.751(20)	O(9) ··· D(2)[a]	1.759(20)	1.78(6)	1.792(17)
O(4) ··· D(3)[a]	2.408(31)	2.16(7)	2.158(22)	O(7) ··· D(4)[b]	2.561(32)	—	2.325(19)
O(4)–D(1) ··· O(9)	175(2)	169(7)	179(2)	O(8)–D(2) ··· O(9)	179(2)	159(6)	179(2)
O(9)–D(3) ··· O(4)	159(3)	160(7)	168(2)	D(1)–O(9)–D(2)	112(1)	—	111(1)
D(1)–O(9) ··· D(3)	122(2)	—	118(1)	D(1)–O(9) ··· D(4)	103(2)	—	105(2)
D(2)–O(9) ··· D(3)	117(2)	—	109(1)	D(3) ··· O(9) ··· D(4)	87(3)	—	103(2)

Note. The values reported from the powder neutron diffraction study, Zr-NPD (3), are given for comparison.
[a] Intralayer H bonds.
[b] Interlayer H bonds.

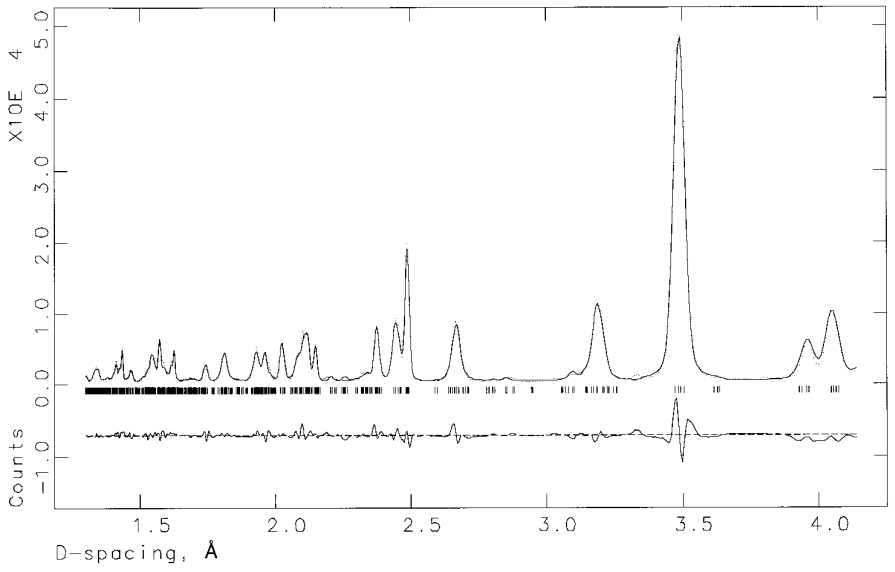

FIG. 5. Final observed (points), calculated (full line), and difference X-ray (λ = 1.5418 Å) profiles for α-$Pb(DPO_4)_2 \cdot D_2O$. Allowed reflection marks are also shown.

hydrogen phosphate groups are slightly longer than those to the remaining oxygens, for both α-ZrP and α-TiP, as exxpected.

One of the objectives of this study was to compare the frameworks of α-ZrP and α-TiP, because in our previous work (7) we concluded that α-ZrP has a larger unit cell than other members of the series. The comparison of the framework bond distances and angles given in Table 4 clearly shows that the M–O–P bonds are more open for α-ZrP than for α-TiP as previously suggested in our X-ray study of α-TiP, α-PbP, and α-SnP (7). Hence, it can be concluded that the α-ZrP layers are less corrugated than those of the other members of the series. In other words, the phosphate tetrahedra are more extruded from the layers for α-MP (M = Ti, Pb, Sn) than for α-ZrP (and Hf). These flat layers in α-ZrP result in more free area per P–OH group. As these groups are the active center in these materials, the high reactivity of α-ZrP is structurally justified.

H-bond network in α-MP series. The deuterium positions derived from this neutron study are similar to those obtained in the previous neutron work (3, 4). However, the better quality of our patterns and the possibility to compare α-ZrP and α-TiP has allowed us to understand better the H-bond network in these materials. First, we have confirmed the two more important H bonds that take place between the deuteriums of the hydrogen phosphate groups, D(1) and D(2), and the oxygen of the water molecule, O(9). These two hydrogen bonds are in the same layer and are linear (Table 5, see Fig. 6). However, our study does not fully agree with the previous neutron work (3) in the intralayer H bond between D(3) and O(4) in α-ZrP. The refined distance is 2.41(3) Å, previously reported as 2.16(7) Å. This intralayer H bond is stronger for a-TiP as evidenced in the refined distance 2.16(2) Å, and it is more linear.

In Fig. 6, the location of the water molecule between two α-MP layers can be seen. The very strong and linear H bonds, O(9)–D(1) and O(9)–D(2), are also displayed. The D(4) of the water molecule points to the center of the zeolitic cavity defined by the three hydrogen phosphate groups but it does not interact strongly with that layer. The H-bond network along the c-axis is slightly different in these materials. It has been confirmed that there are no H bonds between the layers in α-ZrP. The shortest contact is O(7) $\cdots$ D(4), 2.56(3) Å, which is too long to be considered as a hydrogen bond. Hence, the layers in α-ZrP are only held together by van der Waals interactions. However, for α-TiP this contact is much shorter, 2.33(2) Å, which may indicate a small but not negligible H-bond interaction between layers. The results are in full agreement with our early report (7) of a stronger retained water molecule in α-TiP than that in α-ZrP, derived from an IR and thermal study. In the previous study (7) we concluded that α-ZrP was the member of the studied series with the least retained hydration water.

The deuterium environment around the water molecule is a distorted tetrahedron with two short bonds, to D(3) and D(4), and two very long bonds to D(1) and D(2). The angles are quite close to the expected tetrahedral value, 109°, and are more regular for α-TiP than for α-ZrP (Table 5).

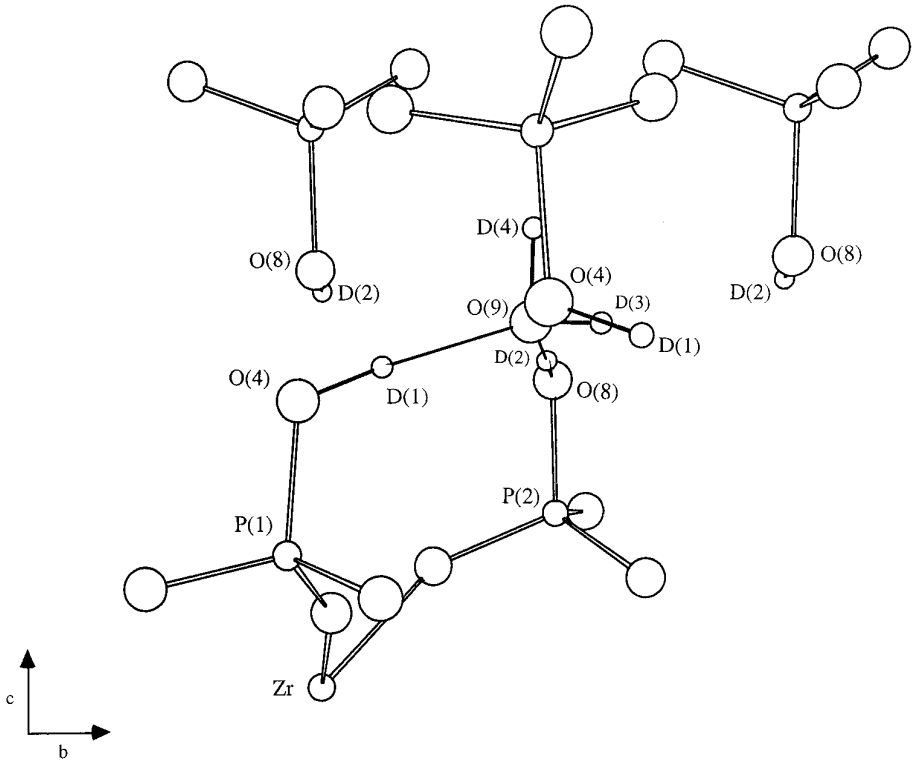

FIG. 6. Location of the water molecule in the interlayer region of α-*MP*, showing the H-bond network. The linear H bonds, O(9)–D(1) and O(9)–D(2), are displayed as narrow solid lines.

There are three main structural characteristics that make α-ZrP a singular, more reactive, and stable host for intercalation reactions. (i) It has more free area per P–OH group, allowing large species to be intercalated. (ii) The layers are flatter improving the accesibility of the guest compounds and minimizing the steric hindrance of the guest–host complex. (iii) The layers are weaker bonded making possible facile intercalation reactions under the same conditions and with similar microparticles sizes. All these structural features make the intercalation chemistry of α-ZrP richer and relatively easier.

CONCLUSIONS

Although acid layered α-*M*P materials have similar crystal structure, some structural differences have been found through combined X-ray and neutron powder diffraction study. There are two main structural differences between α-ZrP and other members of the series. First, the layers in α-ZrP are more flat resulting in more free area per P–OH group. Second, the H-bond network are slightly different. There are no H bonds between the layers, in α-ZrP, which are therefore held together only by van der Waals forces. However in α-TiP, and probably in other members of the series, there is a small but not negligible H-bond interaction between layers.

ACKNOWLEDGMENTS

We thank Dr. Alan Hewat (ILL) for his help during the neutron diffraction experiment (5-22-413), and to ILL for the provision of neutron facilities. This work was supported by DGICYT (Ministerio de Educación y Ciencia, Spain) research grant PB93/1245. E. R. L. thanks the Junta de Andalucía (Spain) for a studentship.

REFERENCES

1. A. Clearfield and G. D.Smith, *Inorg. Chem.* **8,** 431 (1969).
2. J. M. Troup and A. Clearfield, *Inorg. Chem.* **16,** 3311 (1977).
3. J. Albertsson, Å. Oskarsson, R. Tellgren, and J. O.Thomas, *J. Phys. Chem.* **81,** 1774 (1977).
4. A. Christensen, E. K. Andersen, I. G. K. Andersen, G. Alberti, M. Nielsen, and M. S. Lehmann, *Acta Chem. Scand.* **44,** 865 (1990).
5. I. Nakai, K. Imai, T. Kawashima, K. Ohsumi, F. Izumi, and I. Tomita, *Anal. Sci.* **6,** 689 (1990).
6. G. Schuck *et al. Solid State Ionics* **77,** 55 (1995).
7. S. Bruque, M. A. G. Aranda, E. R. Losilla, P. Olivera-Pastor, and P. Maireles-Torres, *Inorg. Chem.* **34,** 893 (1995).
8. T. Hattori, A. Ishiguro and Y. Murakami, *J. Inorg. Nucl. Chem.* **40,** 1107 (1978).
9. A. Clearfield, *in* "Inorganic Ion Exchange Materials." CRC Press, Boca Raton, FL, 1982.
10. G. Alberti, F. Cherubini, and R. Palombari, *Sensors Actuators B* **24–25,** 270 (1995).
11. G. Alberti, *in* "Recent Developments in Ion Exchange" (P. A.

Williams and M. J. Hudson, Eds.). Elsevier Applied Science, Amsterdam, 1987.
12. E. Rodriguez-Castellon, A. Rodriguez, and S. Bruque, *Inorg. Chem.* **24,** 1187 (1984).
13. H. M. Rietveld, *J. Appl. Cryatallogr.* **2,** 65 (1969).
14. A. C. Larson and R. B. Von Dreele, Los Alamos National Laboratory Report No. LA-UR-86-748, 1987.
15. (a) W. A. Dollase, *J. Appl. Cryst.* **19,** 267 (1987); (b) A. March, *Z. Krystallogr.* **81,** 285 (1932).
16. P. Scherrer, *Nachr. Ges. Wiss. Gottingen,* 98 (1918).